

Oriented RepPoints for Aerial Object Detection

Wentong Li, Jianke Zhu, *Senior Member, IEEE*

Abstract—In contrast to the oriented bounding boxes, point set representation has great potential to capture the detailed structure of instances with the arbitrary orientations, large aspect ratios and dense distribution in aerial images. However, the conventional point set-based approaches are handcrafted with the fixed locations using points-to-points supervision, which hurts their flexibility on the fine-grained feature extraction. To address these limitations, in this paper, we propose a novel approach to aerial object detection, named *Oriented RepPoints*. Specifically, we suggest to employ a set of adaptive points to capture the geometric and spatial information of the arbitrary-oriented objects, which is able to automatically arrange themselves over the object in a spatial and semantic scenario. To facilitate the supervised learning, the oriented conversion function is proposed to explicitly map the adaptive point set into an oriented bounding box. Moreover, we introduce an effective quality assessment measure to select the point set samples for training, which can choose the representative items with respect to their potentials on orientated object detection. Furthermore, we suggest a spatial constraint to penalize the outlier points outside the ground-truth bounding box. In addition to the traditional evaluation metric mAP focusing on overlap ratio, we propose a new metric mAOE to measure the orientation accuracy that is usually neglected in the previous studies on oriented object detection. Experiments on three widely used datasets including DOTA, HRSC2016 and UCAS-AOD demonstrate that our proposed approach is effective.

Index Terms—Aerial images, adaptive points learning, oriented object detection, deep learning

I. INTRODUCTION

OBJECT detection is a key technology to semantically understand aerial images, which aims to localize the objects and identify their corresponding class labels. As the fundamental task in remote sensing, it plays an important role in many real-world applications, such as intelligent transportation, maritime surveillance and urban planning [1], [2].

With the prevalence of convolution neural networks (CNNs), object detection in aerial images has achieved substantial progress in recent years. Horizontal bounding box (HBB)-based methods [1], [3]–[5] are straightly derived from the general object detectors, which have difficulties in dealing with the arbitrary orientations and large aspect ratios of the crowded objects in aerial images. To this end, the oriented object detection methods are proposed to fit the spatial regions with different representations of oriented bounding boxes (OBBs) [6]–[8]. As illustrated in Fig. 1-(a), the state-of-the-art oriented detectors [6], [9]–[14] are based on the angle representation using the OBB with five shape parameters including center location, width, height, and rotation angle. Despite promising

Wentong Li and Jianke Zhu are with the College of Computer Science, Zhejiang University, Hangzhou, China, 310027. Jianke Zhu is also with the Alibaba-Zhejiang University Joint Research Institute of Frontier Technologies, Hangzhou, China.

Jianke Zhu is the corresponding author (e-mail: jkzhu@zju.edu.cn).

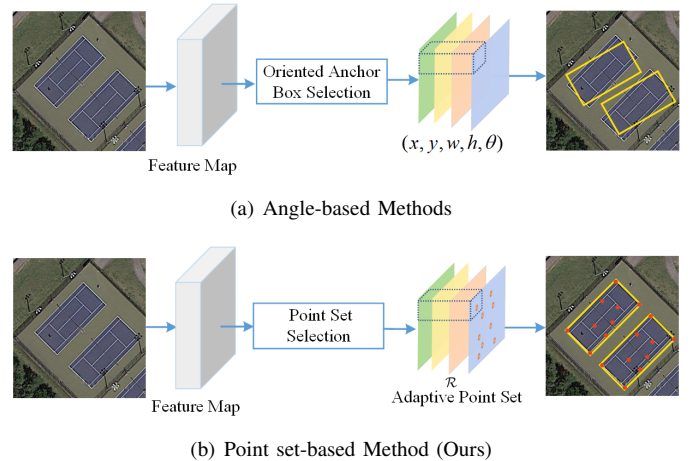


Fig. 1. Comparing to the angle-based methods, our proposed Oriented RepPoints approach achieves more accurate orientation predictions by capturing the fine-grained features. (a) the state-of-the-art methods adopt the angle-based OBB representation regressing the vector (x, y, w, h, θ) and selecting the oriented anchor box in training; (b) our method regresses the adaptive point set \mathcal{R} and chooses the point set in training.

performance, the main showstopper of these methods is the discontinuity of loss due to the periodicity of angle and regression inconsistency, which leads to the instability during training. It may further deteriorate the orientation predictions. Additionally, mean Average Precision (mAP) [15] has been widely used to evaluate the performance of aerial object detector [8], [16], which measures the overlap ratio between the estimated bounding box and ground-truth. However, it mainly focuses on the overlap score while neglecting the orientation differences that is essential to the evaluation on the oriented object detectors.

Being a fine-grained object representation, point set shows the great potential to capture the detailed structure in aerial object detection [16], [17]. Although having obtained encouraging results by conforming the oriented object structure, these point set representations are manually designed with the fixed positions, which limit their generalization capabilities on various orientations with the complicated structure in aerial images. This may lead to the inferior performance. To alleviate this problem, the adaptive points representation are proposed to automatically adjust the displacements locally [18], [19]. These point set-based methods are mainly designed for generic object using an upright-horizontal conversion function like *min-max*, which adopt the conventional anchor box-based metric (i.e., IoU) to select the positive point set samples. This may lose their efficacy for the arbitrary-oriented objects with large aspect ratios and dense distribution in aerial images.

In this paper, we propose a novel approach to aerial object detection, named *Oriented RepPoints*. As shown in Fig. 1-(b),

we take advantage of a set of adaptive points [18] to capture the geometric and spatial information of the arbitrary-oriented, slender and cluttered objects in aerial images, which is able to automatically arrange themselves over the oriented object in a spatial and semantic scenario. Instead of relying on points-to-points supervision, we propose the oriented conversion functions to explicitly transform the point set representation into an oriented bounding box to directly train the detector by ground-truth. Moreover, we introduce an effective quality assessment measure to select the point set samples for training, which can choose the representative items with respect to their potentials on orientated object detection. Furthermore, we suggest a spatial constraint to penalize the outlier points for robust adaptive point set learning. In addition to the traditional evaluation metric focusing on overlap ratio such as mAP, we propose a new metric mAOE to measure the orientation accuracy that is usually neglected in the previous studies on oriented object detection. To the best of our knowledge, there is few work on evaluating the orientation errors that is a key performance indicator for the oriented object detectors. We have conducted the extensive experiments on three widely used datasets, including DOTA [20], HRSC2016 [21] and UCAS-AOD [22], whose promising results demonstrate that our proposed Oriented RepPoints approach is effective for aerial object detection.

Our main contributions are summarized as follows: 1) a set of adaptive points as a fine-grained representation to capture the semantic and geometric information of aerial objects; 2) an effective quality assessment measure to select the representative point set samples for training; 3) a spatial constraint for robust point set learning by penalizing the outliers outside the bounding box; 4) a novel metric to effectively evaluate the orientation accuracy for the oriented object detection.

The rest of this paper is organized as follows. Section II introduces the related works. We give the detailed description of our proposed Oriented RepPoints approach in Section III. Section IV describes the ablation study and experimental results. Finally, Section V concludes this article.

II. RELATED WORK

In this section, we firstly review the related methods on the oriented object detection in aerial images. Then, we investigate the point set representation for object detection. Finally, we study the samples selection strategy in training the object detectors.

A. Oriented Object Detection in Aerial Images

Object detection emerges as an effective tool for aerial images analysis [1], [2], [11], [23]. In general, objects in aerial images are often arbitrary-oriented and dense-distributed with large aspect ratios. To this end, the mainstreamed approaches are directly derived from the general horizontal detectors by introducing different OBB representations, which can be roughly divided into three categories, including angle-based methods [6], [9]–[14], quadrilateral-based approaches [7], [24], [25] and mask-based methods [8], [26].

1) *Angle-based OBBs*: The angle-based methods achieve the state-of-the-art results on aerial object detection, which directly regress five shape parameters including center location, width, height, and rotation angle to obtain the oriented bounding boxes [6], [9]–[11], [11]–[14], [27]. Some approaches [11], [27], [28] preset the oriented anchor boxes with different angles, aspect ratios and scales to better estimate the angle-based OBB. Yang *et al.* [6] regress the horizontal boxes based on a region proposal network (RPN) [29], and then predict the angle-based OBB with an IoU-smooth loss function to tackle the sudden loss change caused by the angular periodicity. To obtain the oriented feature representation, Ding *et al.* [10] present an RoI Transformer to convert horizontal boxes into the oriented boxes. Han *et al.* [12] achieve feature alignment between the oriented objects and axis-aligned features in a full convolutional fashion using a single-stage network. Due to the periodicity of angle and regression inconsistency to the detection metric, these approaches have the difficulties in loss discontinuity. It hurts their robustness, which may lead to the inaccurate prediction on orientation.

2) *Quadrilateral-based OBBs*: The quadrilateral-based approaches employ four vertices of the quadrilateral to represent the oriented objects [7], [24], [25]. Azimi *et al.* [24] directly estimate the four vertices of a quadrilateral to regress an oriented object based on the Image Cascade Network (ICN). Xu *et al.* [7] predict the relative gliding offset of the vertices relative to the four points of horizontal box for the quadrilateral representation, which introduce an obliquity factor to tackle the order confusion of vertices. Qian *et al.* [25] present a modulated loss function by swapping vertices sequence to obtain the better optimization on direction of a quadrilateral. Due to the order confusion of vertices, these methods are not very effective in the case of non-unique quadrilateral definitions, which may fail to eliminate the ambiguity of regression targets.

3) *Mask-based OBBs*: The mask-based methods treat the problem of detecting an oriented object as pixel-level classification [8], [26], which make use of the segmentation map. Wang *et al.* [26] employ the binary segmentation map to locate the oriented objects. Later, Wang *et al.* [8] introduce the center probability map to better represent the oriented objects by reducing the influence of background pixels in aerial images. These methods treat the object detection as a pixel-level segmentation problem, which incurs the computational overheads and requires the pixel-wise labeling.

B. Point Set Representation for Object Detection

Being a flexible and fine-grained object representation, point set has the potential to represent the detailed structures for the accurate classification and localization in object detection.

1) *General Object Detectors*: In general object detection, several studies have already been devoted to developing point set representations in order to address the limitation of bounding boxes in coarse feature extraction and localization [18], [31]–[33]. Wang *et al.* [31] predict the location of four corner points and center point without anchor boxes, and then combine these points to form a bounding box. Law and

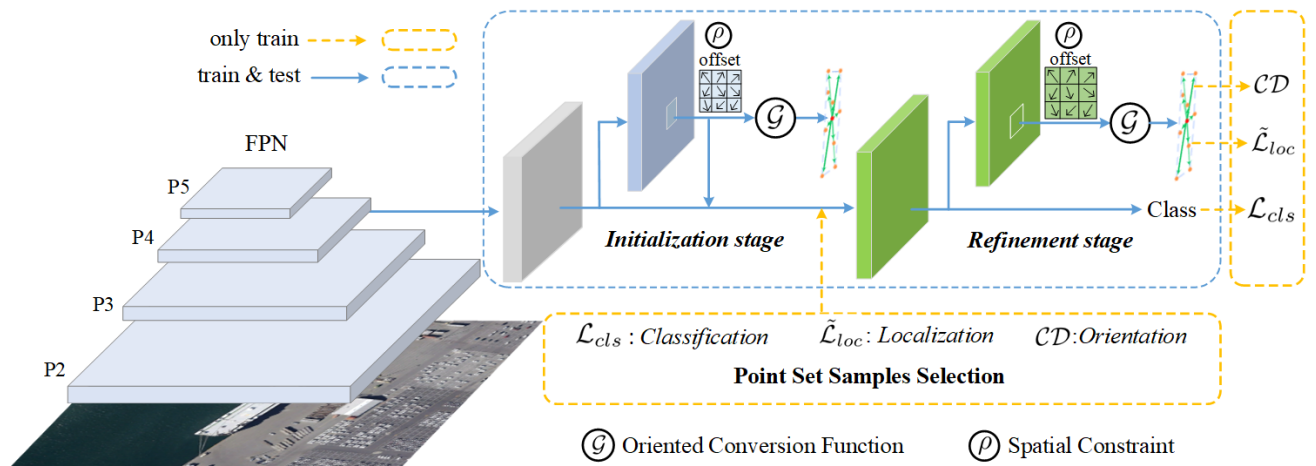


Fig. 2. Our proposed Oriented RepPoints method is an anchor-free approach with the adaptive point set representation, where a backbone network and a feature pyramid network (FPN) [30] are employed for feature extraction. The detection subnetwork consists of two stages for each scale of FPN feature maps. For simplicity, we only visualize the branch of single scale. At the initialization stage, a set of points are regressed from the object center. At the refinement stage, the point set is refined by the selected point set samples according to the presented criteria. The point set sample selection is only performed in training.

Deng [32] predict top-left and bottom-right corner points as a pair of keypoints, which employ a special grouping method to obtain the bounding boxes of objects. Yang *et al.* [18] introduce a set of representative points to describe objects and extracts the point features to capture geometry information. Later, Yang *et al.* [33] regress the center point to estimate the dense points and describe an object at both bounding box level and contour level. These methods are designed for general scenarios, which have achieved promising performance on the COCO dataset [34] and VOC benchmark [15].

2) *Aerial Object Detectors*: Comparing to the general object detectors, there still few point set-based methods for the aerial targets, where the aerial objects have some distinctive characteristics, such as arbitrary orientation, dense distribution and large-aspect ratios with more complicated structures. Wei *et al.* [17] try to employ the endpoints of middle lines and their intersection point to represent an oriented object. Fu *et al.* [16] exploit the four-tuple handcrafted points with the regular layout to represent the objects and achieve points localization based on RPN. Despite the promising classification and localization performance, they show that point set possess great potential to conform the detailed object structure with fine-grained representation. However, these points representation are manually designed with the fixed locations using points-to-points supervision. Differently from these methods, we propose a set of adaptive points as the representation of an oriented object, which can be learned automatically according to the semantic and geometric feature with more flexibility.

C. Sample Selection in Object Detection

It is essential to select the high-quality positive samples in training object detectors. We discuss the traditional strategies in the following two aspects.

1) *Anchor Box Selection*: Under the bounding box-based object detection framework, choosing the high-quality positive samples, *i.e.*, anchor boxes in general object detection or oriented anchor boxes in aerial object detection has been

identified as a pivotal factor to achieve better performance during the training process [35]–[39]. Most of existing object detectors employ the Intersection of Union (IoU) as a matching metric to select the high-quality box samples and assign the label for the supervision of classification and localization. This cannot always guarantee that the selected positive samples are of high-quality with the potential of obtaining accurate detection results, especially for the arbitrary-oriented objects in aerial images. To this end, Zhang *et al.* [35] automatically adjust the IoU threshold according to statistical characteristics in order to adaptively select the high-quality positive samples. Li *et al.* [36] and Kim *et al.* [37] build a score of box samples in classification and localization between its regressed box and ground truth, where PAA [37] formulates the box sample selection as a likelihood maximization with one-dimensional GMM [40].

2) *Sample Selection for Point Set Representation*: Similar to anchor box sample selection, most of point set-based methods firstly convert the learned points into the bounding boxes, and then choose the positive samples based on the IoU metric like those bounding box-based methods [18], [32], [33], [41]. Obviously, these methods ignore the matching degree of point set itself. Based on the adaptive points representation, we suggest a novel quality assessment measure for the positive samples selection of adaptive points from three aspects including classification ability, localization ability and orientation alignment, which greatly improves the discrimination power of high-quality point set samples.

III. ORIENTED REPPOINTS FOR AERIAL OBJECTS

In this section, we firstly give an overview of our proposed method. Then, we introduce the adaptive point set presentation for the arbitrary-oriented object detection. In addition, we describe an effective scheme to select point set samples for training. Finally, we give the details on spatial constraint for robust adaptive point set learning.

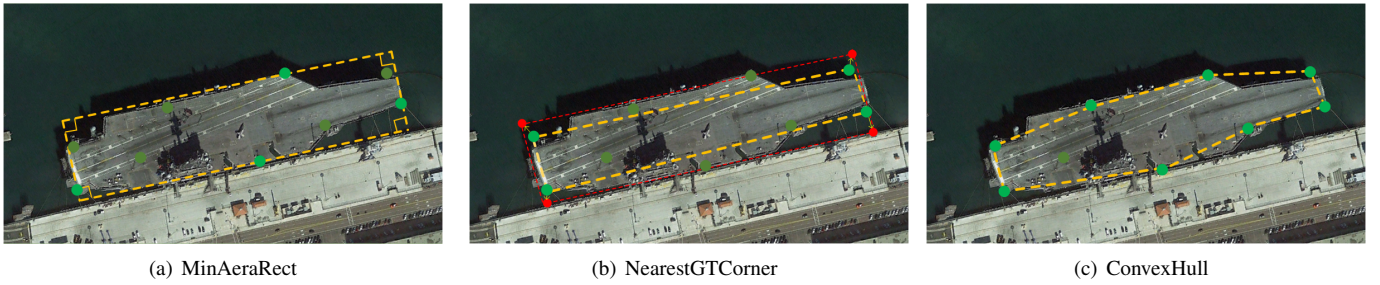


Fig. 3. Illustration of the conversion functions. (a) MinAeraRect. Points in green color are used to get a rotated box with minimum area. (b) NearestGTCorner. Points in red color are GT box corners, and points in green color are selected points with the shortest distance for each GT corners. (c) ConvexHull. Points in green color are used for an oriented polygon.

A. Overview

Differently from the conventional oriented object detection methods, we take advantage of the adaptive point set as a fine-grained representation to capture the key features of the aerial objects with sharp variety on orientation, aspect ratio and cluttered arrangement. Instead of using the points-to-points supervision like previous point-based approach, we employ a differential conversion function to estimate an oriented bounding box from the learned points for the classification and localization, where the representative points are driven to adaptively move toward the appropriate positions over an oriented object. This effectively avoids the ambiguity of regression targets.

As illustrated in Fig. 2, our proposed Oriented RepPoint approach is based on an anchor-free framework, which consists of two stages. The initialization stage regresses the initial point set samples while the refinement stage further gains the accurate point sets. We employ the sample selection scheme to choose the high-quality initial point set for training through an effective quality assessment measure evaluating the initial point set sample from three aspects, such as classification ability, localization ability and orientation alignment. Additionally, we impose the spatial constraints by penalizing the outlier points to ensure that the learned points lie on the object.

B. Adaptive Points Learning for Oriented Object Detector

1) *Adaptive Points-based Representation*: Motivated by the classical anchor-free detector RepPoint [18], the aerial object is represented as a set of adaptive representative points \mathcal{R} :

$$\mathcal{R} = \{\mathbf{p}_1, \dots, \mathbf{p}_n\} \quad (1)$$

where $\mathbf{p}_i = (x + \Delta x_i, y + \Delta y_i)$ denotes the i -th representative point. x and y represent an initial location \mathbf{p} on a feature map. Δx_i and Δy_i are learnable offsets to represent the spatial extent. n is the total number of sample points, which is set to 9 by default in our framework

The horizontal bounding box of a point set can be obtained by a conversion function, such as *min-max*. During the training, the representative points are driven to adaptively move to appropriate locations to represent the object category and accurate position simultaneously.

The representative points in RepPoints [18] enable the network to adaptively capture the key feature of an object.

Nevertheless, we are motivated by the adaptive points learning for arbitrary-oriented objects in opening aerial images with large aspect ratios, dense distribution and more complicated structure, which are challenging to capture its key geometric and semantic information for better performance.

2) *Oriented Object Detector Based on Adaptive points*: To make use of the oriented box annotations for training, we suggest three conversion functions to transform the learned points into oriented box in order to drive the points toward the oriented and slender objects. Let \mathcal{G} denote the oriented conversion function as below:

$$OB = \mathcal{G}(\mathcal{R}) \quad (2)$$

where OB represents an oriented box converted from the learned point set \mathcal{R} . As illustrated in Fig. 3, there are three kinds of conversion function:

- *MinAeraRect* intends to find the rotated rectangle with the minimum area from the learned point set over an oriented object.
- *NearestGTCorner* makes use of the ground-truth annotations. For each corner, we find the closest point from the learned point set as a predicted corner, where the selected corner points are used to build a quadrilateral as the oriented bounding box.
- *ConvexHull*. An oriented instance polygon can be defined as a convex hull of a set of points [42], which is used by many contour-based methods.

3) *Coarse-to-fine Framework*: As shown in Fig. 2, there are two successive stages in our proposed framework. At the initialization stage, the first set of points are regressed from the center of oriented object. Then, the second set of points are estimated as the final location of object at the refinement stage. Based on such scheme, the proposed network achieves the coarse-to-fine progressive prediction with the high localization performance by enjoying the merits of the adaptive point set representation. The oriented boxes OB can be extracted by the conversion function \mathcal{G} at both initialization stage and refinement stage:

$$OB = \mathcal{G}(R_{\mathbf{p}}) \quad (3)$$

where $\mathcal{R} = \{\mathbf{p}_i = (x_i, y_i)\}_{i=1}^n$ is the predicted point set. Let $\mathcal{F}(\mathbf{p})$ denote the feature vector at position \mathbf{p} , which is defined as the concatenation of all representative points of

\mathcal{R} to identify the class of point set. The whole process is formulated as follows:

$$\mathbf{p}_i = \mathbf{p} + \Delta\mathbf{p}_i = \mathbf{p} + T_i(\mathcal{F}(\mathbf{p})) \quad (4)$$

where $\Delta\mathbf{p}_i$ are learnable offsets at the initialization stage, and T_i represents a 2D linear regression function layer to obtain the learned offsets for the oriented objects. Similarly, the predicted position $\tilde{\mathcal{R}} = \{\tilde{\mathbf{p}}_i = (\tilde{x}_i, \tilde{y}_i)\}_{i=1}^n$ can be derived as below:

$$\begin{aligned} \tilde{\mathbf{p}}_i &= \mathbf{p}_i + \Delta\tilde{\mathbf{p}}_i = \mathbf{p} + \Delta\mathbf{p}_i + \Delta\tilde{\mathbf{p}}_i \\ &= \mathbf{p} + \Delta\mathbf{p}_i + \tilde{T}_i(\mathcal{F}(\mathbf{p}_i)) \end{aligned} \quad (5)$$

where $\Delta\tilde{\mathbf{p}}_i$ are corresponding learnable offsets, and \tilde{T}_i is the 2D linear regression function at the refinement stage. Thus, we can obtain the final bounding box estimation OB_i by the conversion function:

$$OB_i = \mathcal{G}(\tilde{\mathcal{R}}_{\tilde{\mathbf{p}}}) \quad (6)$$

Under the presented framework, the semantic key points and geometric points are adaptively learned to capture the detailed structure of an aerial object, which is driven by the localization and classification at the same time rather than point-to-point supervision. In the proposed Oriented RepPoints approach, we aim to minimize the following loss function:

$$\mathcal{L} = \mathcal{L}_c + \lambda_l \mathcal{L}_l + \lambda_s \mathcal{L}_s + \tilde{\lambda}_l \tilde{\mathcal{L}}_l + \tilde{\lambda}_s \tilde{\mathcal{L}}_s. \quad (7)$$

λ_l , λ_s , $\tilde{\lambda}_l$ and $\tilde{\lambda}_s$ are weighting coefficients, which are empirically set to 0.3, 0.05, 1.0 and 0.1, respectively. \mathcal{L}_c denotes the object classification loss:

$$\mathcal{L}_c = \frac{1}{n_{cls}} \sum_i \mathcal{L}_{cls}(\mathcal{R}_i^{cls}(\theta), b_j^{cls}). \quad (8)$$

where $\mathcal{R}_i^{cls}(\theta)$ represents the predicted class confidence, and b_j^{cls} is the assigned ground-truth class. \mathcal{L}_{cls} is the Focal loss [43]. n_{cls} denotes the total number of point set. \mathcal{L}_l represents the localization loss at the initialization stage:

$$\mathcal{L}_l = \frac{1}{n_{loc}} \sum_i [b_j^{cls} \geq 1] \mathcal{L}_{loc}(OB_i^{loc}(\theta), b_j^{loc}). \quad (9)$$

where n_{loc} denotes the number of positive point set samples at the initialization stage, and \mathcal{L}_{loc} is the GIoU loss [44]. b_j^{loc} denotes the location of matched ground-truth box. $\tilde{\mathcal{L}}_l$ is the oriented box localization loss at the refinement stage:

$$\tilde{\mathcal{L}}_l = \frac{1}{\tilde{n}_{loc}} \sum_i [b_j^{cls} \geq 1] \tilde{\mathcal{L}}_{loc}(OB_i^{loc}(\theta), b_j^{loc}) \quad (10)$$

where \tilde{n}_{loc} is the total number of selected positive point set. \mathcal{L}_s and $\tilde{\mathcal{L}}_s$ are the spatial constraints defined in Section III-D for the initialization and refinement stage, respectively.

C. Sample Selection for Point Set Representation

In our proposed Oriented RepPoints framework, the initial point set samples are regressed based on the center of objects. Since the refinement stage is dependent on the selected samples from the initialization stage, whose quality is essential to the final detection results. To this end, we suggest an effective measure to evaluate the quality of the initial point set samples. It is worthy of mentioning that selecting point set samples is only performed in training, which does not incur the computational load at the inference stage.

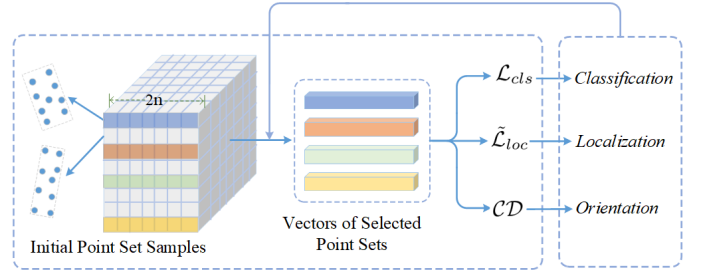


Fig. 4. The scheme of choosing the initial point set samples during the training.

1) Quality Assessment Measure of Point Set Samples:

Due to the large variations on orientation and aspect ratio in aerial objects, we define a quality assessment measure Q to evaluate the initial point set samples from three aspects, including classification ability Q_{cls} , localization ability Q_{loc} , and orientation alignment Q_{ori} . We define Q as below:

$$Q = Q_{cls} + \mu Q_{loc} + \beta Q_{ori} \quad (11)$$

where μ is empirically set to 1, and β is 0.3.

The classification ability Q_{cls} of a point set \mathcal{R}_i is directly reflected by its classification confidence $\mathcal{R}_i^{cls}(\theta)$, where the corresponding classification loss \mathcal{L}_{cls} measures the compatibility of the points feature with ground-truth class b_j^{cls} . We define Q_{cls} as follows:

$$Q_{cls}(\mathcal{R}_i, b_j) = \mathcal{L}_{cls}(\mathcal{R}_i^{cls}(\theta), b_j^{cls}) \quad (12)$$

For the localization ability Q_{loc} of a point set \mathcal{R}_i , we convert its predicted point set $\mathcal{R}_i^{loc}(\theta)$ into an oriented box $OB_i^{loc}(\theta)$ by the conversion function \mathcal{G} :

$$OB_i^{loc}(\theta) = \mathcal{G}(\mathcal{R}_i^{loc}(\theta)) \quad (13)$$

Similar to the bounding box-based methods, IoU between OB_i^{loc} and the ground-truth b_j^{loc} is closely related with the spatial alignment when the center of a point set is near to the geometric center of object. To evaluate the compatibility of the points position with ground-truth b_j^{loc} , we employ the localization loss as the quality assessment measure, which is equal to the negative logarithm of IoU score. Therefore, Q_{loc} is defined as below:

$$\begin{aligned} Q_{loc}(\mathcal{R}_i, b_j) &= -\log(\text{IoU}(OB_i^{loc}(\theta), b_j^{loc})) \\ &= \tilde{\mathcal{L}}_{loc}(OB_i^{loc}(\theta), b_j^{loc}) \end{aligned} \quad (14)$$

IoU can be regarded as a similarity measure that reflects the distance between the center of point set and the object. However, it is insensitive to the orientation variations. Thus, IoU is not an effective measure to evaluate the orientation alignment between the predicted point set and object. To account for the orientation alignment, we employ *Chamfer distance* [45] to measure the difference in orientation between the predicted point set and ground-truth.

As shown in Fig. 5, we firstly adopt the *NearstGTCorner* conversion function to select four corner points $\{v_1, v_2, v_3, v_4\}$ from the predicted point set. Then, an ordered point set \mathcal{R}^v is sampled with the equal interval from two adjacent corner points. We sample 40 points for each point set by default.

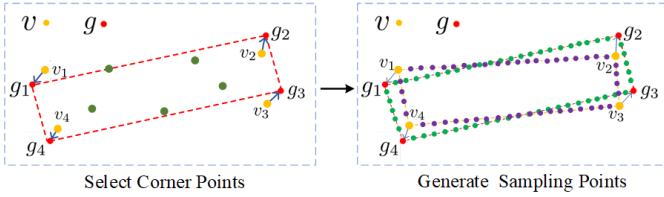


Fig. 5. The process of sampling points with respect to the bounding box. Red points denote the ground-truth corner points, and yellow points represent the selected corner points from the predicted point set. The purple points and green points are the sampled points for prediction and ground truth, respectively.

Similarly, the points \mathcal{R}^g are generated for the ground-truth corner points $\{g_1, g_2, g_3, g_4\}$. Therefore, Q_{ori} is defined as follows:

$$Q_{ori}(\mathcal{R}_i, b_j) = \mathcal{CD}(\mathcal{R}_i^v(\theta), \mathcal{R}_{b_j}^g) \quad (15)$$

where \mathcal{CD} denotes Chamfer distance between the predicted bounding box and ground truth:

$$\begin{aligned} \mathcal{CD}(\mathcal{R}^v, \mathcal{R}^g) &= \frac{1}{2n} \sum_{i=1}^n \min_j \| (x_i^v, y_j^v) - (x_i^g, y_j^g) \|_2 \\ &+ \frac{1}{2n} \sum_{j=1}^n \min_i \| (x_i^v, y_j^v) - (x_i^g, y_j^g) \|_2 \end{aligned} \quad (16)$$

$(x_i^v, y_j^v) \in \mathcal{R}^v$ denotes the sampled points of predicted corner points, and $(x_i^g, y_j^g) \in \mathcal{R}^g$ denotes the sampled points generated from ground-truth corner points.

2) *Initial Point Set Sample Selection*: Based on the quality assessment measure Q , we choose the initial point set samples through an efficient top k item selection scheme. For each oriented object, we first sort all the initial point set samples according to their quality assessment scores. To retrieve high-quality initial point set samples, we set a sampling ratio σ to select the top k samples with the smallest quality measures, which is calculated by:

$$k = \sigma * n_{tot} \quad (17)$$

where n_{tot} denotes the total number of initial point set samples for each oriented object.

During the training phase, the selected samples are regarded as the positive items while the remaining ones are treated as the negative samples. Thus, the high-quality points samples can be chosen according to the quality assessment measure Q . All the initial point set samples are assigned with the class label of foreground or background, and only the selected positive point sets are assigned with the ground-truth bounding box of target.

D. Spatial Constraint for Adaptive Points Learning

Instead of relying on the point-to-point supervision with the fixed positions, the adaptive points learning tends to choose the keypoints with the strong features. Due to the diversity of categories and the complex background in aerial images, a portion of learned points are likely outside the ground-truth bounding box, as depicted in Fig. 6. These outliers sample the features in the background or adjacent objects, which may not

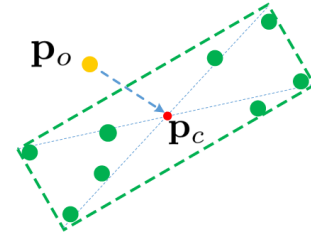


Fig. 6. Green dashed line denotes the boundary of ground-truth box, in which the red point is its geometric center. Green points represent the learned point set inside the ground-truth bounding box while yellow ones are outlier points outside. Blue dashed line denotes the penalty to constrain the outlier points in order to capture the actual feature inside the bounding box.

truly represent the target. To effectively capture the semantic features on an oriented object, we suggest a spatial constraint to penalize those sampled points outside the bounding box in the proposed adaptive point set learning process. Let \mathbf{p}_c denote the geometric center of the ground-truth bounding box. Given a sampled outlier point \mathbf{p}_o outside the bounding box, we employ the Euclidean distance between \mathbf{p}_o and \mathbf{p}_c as a penalty to prevent the points drifting far away from their center. Therefore, the spatial loss \mathcal{L}_s for an instance can be derived as below:

$$\mathcal{L}_s = \sum_{i=1}^n \rho_i \quad (18)$$

where ρ_i represents the cost for each point:

$$\rho_i = \begin{cases} \|\mathbf{p}_i - \mathbf{p}_c\|, & \mathbf{p}_i \text{ is outside } GT \\ 0, & \text{otherwise.} \end{cases} \quad (19)$$

where GT denotes the ground-truth box. Fig. 8 shows some exemplar results of the learned adaptive point set. It can be clearly observed that our proposed approach is able to effectively find the semantic keypoints on an oriented objects.

IV. EXPERIMENTS

In this section, we present our experimental setup and implementation details. Moreover, we perform a series of ablation study to examine the effectiveness of the proposed method. Furthermore, we compare our method with the recent state-of-the-art approaches on aerial object detection.

A. Experiment Setup

1) *Dataset*: To investigate the effectiveness of our proposed arbitrary-oriented object detector, we perform the extensive experiments on three widely used datasets on aerial object detection, including DOTA [20], HRSC2016 [21] and UCAS-AOD [22]. The annotations of these datasets are oriented bounding boxes.

DOTA [20] is a large-scale dataset to evaluate the detection performance of oriented objects in aerial images, which contains 2806 images, 188,282 instances and 15 categories with a variety of orientations, scales, and shapes. The whole dataset is partitioned into three parts. The training set is with 1411 images while the validation set is with 458 images. Testing set is made of 937 images. The images size ranges from 800×800 to 4000×4000 . In our experiments, both the training set

and validation set are employed to train the proposed detector, and the testing set without annotations is used for evaluation. As in [12], we crop the original images into the patches of 1024×1024 with a stride of 824. At the training stage, we employ random resizing in order to avoid over-fitting. Moreover, random rotation is used for data augmentation to facilitate the fair comparisons. For the evaluation on multi-scale data augmentation, the original images are resized at three scales $\{1.5, 1.0$ and $0.5\}$, from which the patches of 1024×1024 are cropped with a stride of 500.

HRSC2016 [21] is a challenging high-resolution remote sensing dataset collected from several famous harbors for ship recognition, which has a large number of strip-like oriented objects with diverse appearances. The entire dataset contains 1061 images ranging from 300×300 to 1500×900 . The training set, validation set and testing set have 436, 181 and 444 images, respectively. For a fair comparison, both the training set and validation set are used for training in our experiments.

UCAS-AOD [22] is an aerial image dataset for small object detection, including car and airplane. It involves 1510 images with 510 car images and 1000 airplane images. There are 14,596 instances in total. The entire dataset is randomly divided into 755 images for training, 302 images for validation and 453 images for testing with a ratio of 5:2:3. The size of all images is approximately 1280×659 .

2) *Evaluation Metric*: In addition to the traditional evaluation metric *mean Average Precision* (mAP) on overlap ratio [8], [16], [46], we suggest a novel measure *mean Average Orientation Error* (mAOE) to take into consideration of the orientation differences for the arbitrary-oriented object detectors. To represent the object orientation, we define the angle θ between the edge of bounding box and the positive direction of horizontal axis, which is similar to the angle-based methods [12]. Thus, we compute the Average Orientation Error (AOE) for each category as follows:

$$\text{AOE} = \frac{1}{n_p} \sum_i |\theta_i^{GT} - \theta_i^{Det}| \quad (20)$$

where n_p denotes the total number of instances. θ^{GT} and θ^{Det} denote the angle ($^\circ$) of ground-truth and detected bounding box, respectively. Therefore, mAOE is the mean value of AOE on all categories:

$$\text{mAOE} = \frac{1}{n_c} \sum_i \text{AOE}_i \quad (21)$$

where n_c is the total number of categories. Smaller the mAOE value, the better orientation prediction is.

With two pairs of parallel edges in a rectangle, a straightforward definition on rotation angle has ambiguity. To deal with this problem, we suggest to use the long edge w to calculate the angle, as shown in Fig. 7-(a). For the nearly squared bounding box, such definition may lead to large errors, as illustrated in Fig. 7-(c). To avoid this issue, we choose the smallest angle between two adjacent edges for the nearly squared object, as shown in Fig. 7-(b). Practically, we treat a bounding box as the nearly squared one when its aspect ratio ε is less than a given threshold 1.15.

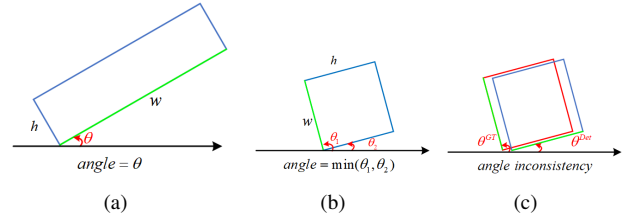


Fig. 7. Angle definition for oriented bounding box, where w and h denote the long edge and short edge, respectively. The aspect ratio ε is equal to w/h . (a) the angle of rectangle objects with $\varepsilon \geq 1.15$; (b) denotes the angle for nearly squared objects when $1.0 \leq \varepsilon < 1.15$; (c) shows the angle inconsistency between the detected box (blue color) and ground-truth (red color) for the nearly squared bounding box.

3) *Implementation Details*: In the ablation study, we employ ResNet-50 [47] as the backbone network. To compare the state-of-the-art approaches, we implement our proposed approach on both ResNet-50 and ResNet-101. The FPN [30] consists of P_3 to P_7 pyramid levels in our network. The stochastic gradient descent (SGD) optimizer is used in training. The initial learning rate is set to 0.01 with the warming up for 500 iterations, and the learning rate is decreased by a factor of 0.1 at each decay step. The momentum and weight decay are set to 0.9 and 0.0001, respectively. We train the models with 40, 120, 120 epochs for DOTA, HRSC2016 and UCAS-AOD, respectively. The hyperparameters of focal loss \mathcal{L}_{cls} are set to $\alpha = 0.25$ and $\gamma = 2.0$. A couple of experiments are run to choose the appropriate values of the sampling ratio σ with point set samples selection in Table III. We conduct the experiments on a server with 8 RTX 2080Ti GPUs using a total batch size of 16 (2 images per GPU) for training. We use a single RTX 2080Ti GPU for inference.

B. Ablation Study

To investigate the effectiveness of the adaptive point set representation, we perform a series of ablation study on DOTA [20] dataset. It is worth noting that only the mAP metric is used in the ablation experiments for simplicity.

1) *Evaluation on Oriented Conversion Functions*: The conventional point set-based object detector RepPoints [18] only takes consideration of the upright bounding boxes by using square conversion function, such as *min-max*, which cannot deal with the aerial objects having arbitrary orientations. Therefore, a straightforward implementation will lead to poor performance. To build a reasonable baseline, we compare the different conversion functions that map the adaptive points into the oriented box during the training and evaluation. In the proposed conversion functions, both *NearestGTCorner* and *ConcaveHull* functions are differentiable, which are able to be used in training. On the contrary, *MinAeraRect* function is not differentiable, which can only be employed as the post-processing method estimating the oriented box for performance evaluation.

Table I shows the comparison results. It can be seen that the proposed *ConvexHull* conversion function with *MinAeraRect* post processing achieves the best result, which can make full use of all learned points to obtain a surrounding polygon of instance. Note that the conventional method [18] employs

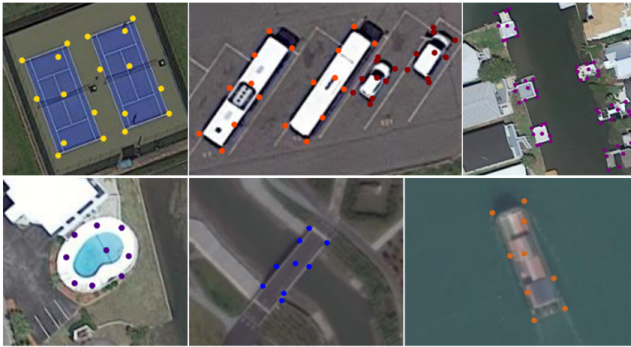


Fig. 8. Examples of the learned points on DOTA dataset, which are usually located at the semantic keypoints of an oriented objects.

min-max conversion function in both training and testing. It performs poor with 49.69% mAP on the task of locating aerial objects, which indicates that the simple *min-max* method is not suitable for the challenging task of detecting objects in aerial images. Furthermore, *ConvexHull* approach performs better than *NearestGTCorner* method that only uses the four nearest corner points for supervision. In the following, we employ the *ConvexHull* conversion function with *MinAeraRect* post processing as the strong baseline for evaluation.

TABLE I
PERFORMANCE COMPARISONS OF THE DIFFERENT CONVERSION FUNCTIONS ON DOTA DATASET(%).

Training	Post-processing	mAP
<i>min-max</i>	<i>min-max</i>	49.69
<i>min-max</i>	<i>MinAeraRect</i>	53.21
<i>NearestGTCorner</i>	<i>MinAeraRect</i>	66.97
<i>ConvexHull</i>	<i>MinAeraRect</i>	68.89

TABLE II
PERFORMANCE OF SPATIAL CONSTRAINT ON DOTA DATASET (%).

Spatial Constraint	BD	BR	RA	HC	mAP
✓	76.85 79.99	41.72 45.33	67.09 71.39	41.55 51.87	68.89 70.11

2) *Evaluation on Spatial Constraint*: To examine the effectiveness of our proposed spatial constraint, we compare it against the baseline method without it. Table II shows the experimental results. It can be observed that our proposed method achieves better performance comparing to the baseline method without using the spatial constraint. This indicates that penalization on the outside points are beneficial for the point set-based detector. Moreover, we give the results of the categories with the significant improvements. The performance of BD (Baseball Diamond), BR (Bridge) and RA (Roundabout) are greatly affected by the complex background noise. With our proposed spatial constraint, the results of these categories are improved by +3.14%, +3.61% and +4.30% AP, respectively. More importantly, our proposed method outperforms the baseline method at a very large margin of +10.32% mAP on HC (Helicopter). This is because the helicopter is too thin

to be captured by the adaptive point set learning, where the points can easily move outside the bounding box without the spatial constraint.

TABLE III
EVALUATION ON VARIOUS σ IN POINT SET SAMPLES SELECTION ON DOTA DATASET (%).

α	0.2	0.3	0.4	0.5
	75.45	75.34	75.68	75.67

TABLE IV
PERFORMANCE EVALUATION ON DIFFERENT SETTINGS OF QUALITY ASSESSMENT MEASURE IN POINT SET SAMPLES SELECTION ON DOTA DATASET(%).

	Different settings of Q			
	✓	✓	✓	✓
Q_{cls}				
Q_{loc}				
Q_{ori}				
	70.11	72.67	75.03	75.68

TABLE V
PERFORMANCE COMPARISON OF DIFFERENT POSITIVE SAMPLES SELECTION METHODS ON DOTA DATASET(%).

Methods	mAP
MaxIoU [29]	70.11
ATSS [35]	72.87
PAA [37]	74.62
Oriented RepPoints (ours)	75.68

3) *Evaluation on Positive Samples Selection*: Choosing positive point set samples plays a key role in training the high-performance aerial object detector. We firstly study the influence of sampling ratio σ . Secondly, we analyse the effectiveness of our proposed quality assessment measure. Finally, we compare the arbitrary-oriented object detection results with different positive samples selection schemes in training.

Under the presented framework, the total number of selected point set samples is determined by the sampling ratio σ . We run a group of experiments with different values of σ . As shown in Table III, the model achieves the best performance of 75.68% mAP when $\sigma = 0.4$.

As the quality assessment measure Q is composed of three terms, including classification ability Q_{cls} , localization ability Q_{loc} and orientation alignment Q_{ori} . Table IV gives the results of different settings on quality assessment measure when the sampling ratio $\sigma = 0.4$. By taking into consideration of classification ability Q_{cls} only, it achieves 72.67% mAP with 2.56% improvement compared with the base 70.11%. When both classification and localization terms are employed, it achieves 75.03% mAP with 4.92% improvement. The model using all three terms achieves the best performance with 75.68% mAP. It implies that the proposed quality assessment measure is effective for adaptive point set learning.

We study the arbitrary-oriented object detection results with different positive samples selection schemes for training, including MaxIoU [29], ATSS [35], PAA [37] and our proposed

TABLE VI
RESULTS ON THE OBB TASK OF DOTA DATASET. 'T', 'S' AND 'A' INDICATE TWO-STAGE, SINGLE-STAGE AND ANCHOR-FREE METHODS, RESPECTIVELY. R-50, R-101, R-152 AND H-104 DENOTE THE BACKBONE OF RESNET-50, RESNET-101, RESNET-152 AND HOURGLASS-104, RESPECTIVELY. 'MS' REPRESENTS THE MULTI-SCALE TRAINING AND TESTING(%).

Methods	Backbone	Type	MS	PL	BD	BR	GTF	SV	LV	SH	TC	BC	ST	SBF	RA	HA	SP	HC	mAP
OBB-Based Methods																			
FR-O [20]	R-101	T		79.09	69.12	17.17	63.49	34.20	37.16	36.20	89.12	69.60	58.96	49.4	52.52	46.69	44.80	46.30	52.93
ICN [24]	R-101	T		81.36	74.30	47.70	70.32	64.89	67.82	69.98	90.76	79.06	78.20	53.64	62.90	67.02	64.17	50.23	68.16
RetinaNet [43]	R-101	S		88.82	81.74	44.44	65.72	67.11	55.82	72.77	90.55	82.83	76.30	54.19	63.34	63.71	69.73	53.37	68.72
CAD-Net [9]	R-101	T		87.80	82.40	49.40	73.50	71.10	63.50	76.60	90.90	79.20	73.30	48.40	60.90	62.00	67.00	62.20	69.90
SCRDet [6]	R-101	T		89.98	80.65	52.09	68.36	68.36	60.32	72.41	90.85	87.94	86.86	65.02	66.68	66.25	68.24	65.21	72.61
R ³ Det [27]	R-101	S		88.76	83.09	50.91	67.27	76.23	80.39	86.72	90.78	84.68	83.24	61.98	61.35	66.91	70.63	53.94	73.79
S ² A-Net [12]	R-50	S		89.11	82.84	48.37	71.11	78.11	78.39	87.25	90.83	84.90	85.64	60.36	62.60	65.26	69.13	57.94	74.12
RoI-Trans. [10]	R-101	T	✓	88.64	78.52	43.44	75.92	68.81	73.68	83.59	90.74	77.27	81.46	58.39	53.54	62.83	58.93	47.67	69.56
DRN [48]	H-104 [49]	A	✓	89.71	82.34	47.22	64.10	76.22	74.43	85.84	90.57	86.18	84.89	57.65	61.93	69.30	69.63	58.48	73.23
MFIAR-Net [13]	R-152	T	✓	89.62	84.03	52.41	70.30	70.13	67.64	77.81	90.85	85.40	86.22	63.21	64.14	68.31	70.21	62.11	73.49
Gliding Vertex [7]	R-101	T	✓	89.64	85.00	52.26	77.34	73.01	73.14	86.82	90.74	79.02	86.81	59.55	70.91	72.94	70.86	57.32	75.02
BBAVecotors [50]	R-101	A	✓	88.63	84.06	52.13	69.56	78.26	80.40	88.06	90.87	87.23	86.39	56.11	65.62	67.10	72.08	63.96	75.36
FFA-3 ⁺⁺ [11]	R-101	T	✓	90.10	82.70	54.20	75.20	71.00	79.90	83.50	90.70	83.90	84.60	61.20	68.00	70.70	76.00	63.70	75.70
MaskOBB [26]	R-50	T	✓	89.60	85.82	56.50	71.18	77.62	70.45	85.04	90.18	80.10	85.30	56.60	69.43	75.45	76.71	69.70	75.98
CenterMap [8]	R-101	T	✓	89.83	84.41	54.60	70.25	77.66	78.32	87.19	90.66	84.89	85.27	56.46	69.23	74.13	71.56	66.06	76.03
S ² A-Net [12]	R-101	S	✓	89.28	84.11	56.95	79.21	80.18	82.93	89.21	90.86	84.66	87.61	71.66	68.23	78.58	78.20	65.55	79.15
Point Set-Based Methods																			
O ² -DNet [17]	H-104	A		89.31	82.14	47.33	61.21	71.32	74.03	78.62	90.76	82.23	81.36	60.93	60.17	58.21	66.98	61.03	71.04
FR-Est-FPN [16]	R-101	T		89.63	81.17	50.44	70.19	73.52	77.98	86.44	90.82	84.13	83.56	60.64	66.59	70.59	66.72	60.55	74.20
Oriented RepPoints (Ours)	R-50	A		86.95	80.84	53.20	70.50	80.85	79.35	87.36	90.88	85.95	85.60	61.12	70.08	73.43	72.58	56.46	75.68
Oriented RepPoints (Ours)	R-101	A		89.21	84.22	58.42	72.05	79.81	77.66	87.35	90.87	87.10	84.80	61.79	67.76	73.89	73.38	54.75	76.21
FR-Est-FPN [16]	R-101	T	✓	89.77	85.16	55.32	76.47	80.08	83.26	87.53	90.61	87.36	86.89	65.09	68.48	71.63	79.60	66.10	77.62
Oriented RepPoints (Ours)	R-101	A	✓	88.72	80.56	55.69	75.07	81.84	82.40	87.97	90.80	84.33	87.64	62.80	67.91	77.69	82.94	65.46	78.12

TABLE VII
ORIENTATION ESTIMATION RESULTS ON DOTA VALIDATION SET. R-50 DENOTES THE BACKBONE OF RESNET-50(°).

Methods	Backbone	PL	BD	BR	GTF	SV	LV	SH	TC	BC	ST	SBF	RA	HA	SP	HC	mAOE
RetinaNet [43]	R-50	16.21	28.70	5.35	2.86	4.39	3.34	3.22	1.92	2.55	23.99	2.90	21.35	4.56	7.25	14.39	9.53
RoI-Trans. [10]	R-50	13.19	14.91	5.31	2.69	4.80	3.05	4.80	1.76	2.46	5.76	2.27	7.99	2.81	8.03	20.46	6.70
S ² A-Net [12]	R-50	20.45	26.07	6.51	6.62	6.11	4.95	5.81	3.08	5.02	16.29	4.94	19.63	5.97	9.87	15.26	11.19
Oriented RepPoints (Ours)	R-50	12.39	11.25	7.51	3.29	4.56	3.51	5.53	1.10	1.70	5.12	1.36	6.73	3.12	8.74	13.08	5.93

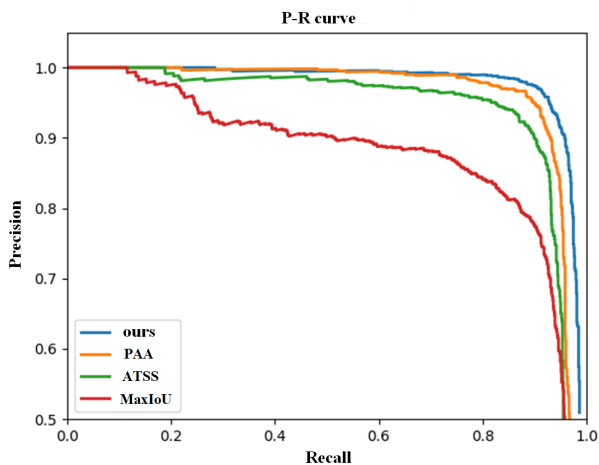


Fig. 9. Precision-recall curve on the testing set of HRSC2016.

approach. MaxIoU selects the positive samples based on IoU metric with a fixed threshold, which is used in RepPoints [18]. ATSS chooses the appropriate positive samples with a dynamic IoU threshold that is based on the statistical characteristics

of objects. PAA selects the positive samples based on the probability distribution of sample's scores and maximize the likelihood with a complex GMM procedure of two modalities, which are optimized by Expectation-Maximization (EM) algorithm [51]. Table V shows the performance comparisons on DOTA dataset. It can be found that our proposed sample selection scheme performs the best on DOTA dataset. Comparing to the baseline MaxIoU method, we obtain the improvement of 5.57% mAP. Both PAA and our proposed approach perform better than the IoU thresholding methods like MaxIoU and ATSS. It is mainly due to the fact that IoU-based selection criteria tends to choose the samples close to the objects' geometric center without enough sensitivity on orientation difference. Additionally, our method outperforms the PAA method, which indicates that the classification score, localization ability and orientation alignment are important performance metrics for arbitrary-oriented object detection. Moreover, choosing the top k samples is more efficient than the time-consuming GMM method in PAA. To further analyze the performance on different positive sample selection methods, we plot the precision-recall curve on HRSC2016 dataset [21] in Fig. 9, which demonstrates that our proposed sample selection scheme is more effective.

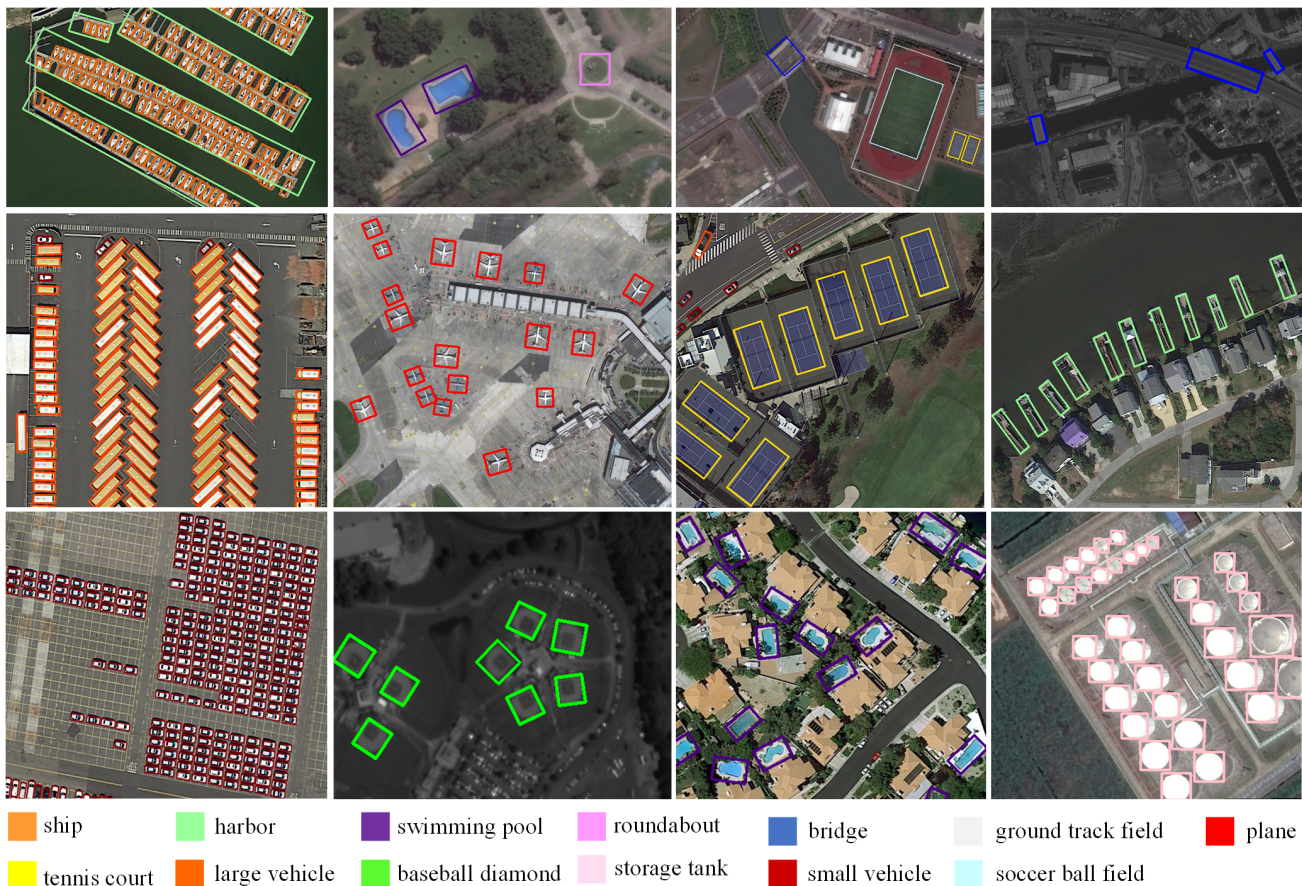


Fig. 10. Sample object detection results of our proposed Oriented RepPoints method on DOTA.

TABLE VIII

RESULTS ON HRSC2016 TEST SET. mAP_{07} AND mAP_{12} REPRESENTS THE REPORTED RESULTS UNDER VOC2007 AND VOC2012 MAP METRICS(%). THE MAOE IS THE ORIENTATION RESULTS($^{\circ}$).

Methods	mAP_{07}	mAP_{12}	MAOE
RC1 & RC2 [21]	75.70	-	-
R ² PN [52]	79.60	-	-
RRPN [53]	79.08	85.64	-
RRD [54]	84.30	-	-
RoI-Trans. [10]	86.20	-	1.64
Gliding Vertex [7]	88.20	-	-
DRN [48]	-	92.70	-
CenterMap-Net [8]	-	92.80	-
R ³ Det [27]	89.26	96.01	-
Fu <i>et al.</i> [16]	89.70	-	-
S ² A-Net [12]	90.17	95.01	2.51
Oriented RepPoints (Ours)	90.38	97.26	1.29

C. Comparisons with the State-of-the-Art Methods

To further investigate the performance of aerial object detection, we compare our proposed method against the state-of-the-art approaches on three benchmark datasets including DOTA [20], HRSC2016 [21] and UCAS-AOD [22].

1) *Results on DOTA*: DOTA is the de-facto standard benchmark dataset for the oriented object detection. For the sake of fair comparison, data augmentation is adopted. The images are rotated with an angle selected from $\{30^{\circ}, 60^{\circ}, 90^{\circ}, 120^{\circ},$

TABLE IX

RESULTS OF $MAP(\%)$ AND $MAOE(^{\circ})$ PERFORMANCE ON UCAS-AOD DATASET.

Methods	car	airplane	AP ₅₀	AP ₇₅	MAOE
YOLOv3 [55]	74.63	89.52	82.08	-	-
RetinaNet [43]	84.64	90.51	87.57	-	-
FR-O [20]	86.87	89.86	88.36	47.08	4.62
RoI Trans. [10]	87.99	89.90	88.95	50.54	1.83
Oriented RepPoints (Ours)	89.51	90.70	90.11	56.75	1.61

150° } randomly in the training phase. Specifically, we resize the original images at three scales before dividing the images into the patches with the size of 1024×1024 for multi-scale training and testing experiments.

We firstly evaluate the performance on the overlap ratio between bounding boxes. As shown in Table VI, we compare our proposed method with the state-of-the-art approaches with different representations, i.e., OBB-based methods and point set-based methods. With the ResNet-50 backbone, our method achieves the best result of 75.68% mAP without data augmentation, which outperforms the angle-based method S²A-Net [12] over 1.56% mAP. This demonstrates the effectiveness of our method. As for the point set-based methods, the proposed method obtains 76.21% mAP with ResNet-101 backbone with random rotation on the original dataset, which outperforms O²-DNet [17] and FR-Est-FPN [16] with 5.17%

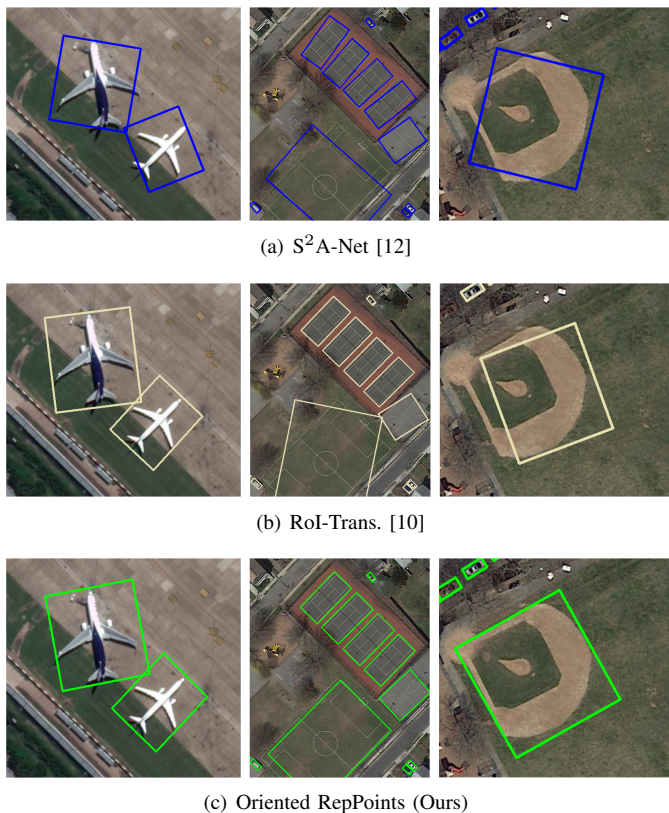


Fig. 11. Visual comparison of orientation performance on validation dataset of DOTA. (a) denotes the visual results (blue color) of S²A-Net [12]. (b) represents the visual results (tawny color) of RoI-Trans. [10]. (c) represents the visual results (green color) of our method .

mAP and 2.01% mAP. In the case of multi-scale training and testing, we achieve the second best result with 78.12% mAP, which is a bit weaker than S²A-Net and outperforms point set-based FR-Est-FPN [16] with 0.50% mAP. For small objects with dense distribution, such as small vehicle (SV) and storage tank (ST), our method achieves 81.84% AP and 87.64% AP. The swimming pool (SP) with irregular shape in DOTA, our adaptive points-based method achieves the best performance with 82.94% AP, which outperforms the second place over 3.34% AP. These results demonstrate that the adaptive point set has much potential in capturing the fine-grained feature. Some visual results on the DOTA dataset are illustrated in Fig. 10.

For the evaluation on orientation error, Table VII shows the results. Due to the lack of labels for the testing set of DOTA dataset [20], we compare the state-of-art methods with our methods on its validation set. With the ResNet-50 backbone, our method achieves the lowest mAOE among the various approaches. Our method obtains the best orientation prediction results on plane (PL), baseball diamond (BD), tennis court (TC), basketball court (BC), storage tank (ST), soccer-ball field (SBF), roundabout (RA) and helicopter (HC) categories. Comparing to the angle-based methods, our approach is based on the adaptive point set learning, which does not introduce the sensitive parameters like rotation angle. Besides, we employ the quality assessment measure to choose the representative point set samples with the accurate orientation during train-

ing. Therefore, our method is able to accurately predict the orientation of aerial object. Fig. 11 shows the visual results.

2) *Results on HRSC2016*: The HRSC2016 dataset contains plenty of strip-like ship objects with arbitrary orientations. We compare our proposed Oriented RepPoints method with the recent approaches on this dataset. Since some methods are evaluated under VOC2007 metric, others are compared under VOC2012 metric. To make a comprehensive comparison, we report the results with the both metrics. Table VIII shows the experimental results. Using the ResNet-50 backbone, our methods achieves the best performance with 90.38% mAP under VOC2007 metric and 97.26% mAP under VOC2012 metric. Most of OBB-based methods often employ many rotated anchors to achieve accurate orientation prediction, like RoI-Trans. [10] and R³Det [27], which incurs heavy computational cost. Compared with the state-of-the-art approaches, such as angle-based S²A-Net [12], handcrafted points-based FR-Est-FPN [16], our proposed method achieves better performance by taking advantage of the adaptive point set learning with accurate orientations. This demonstrates the efficacy of our proposed approach on arbitrary-oriented object detection in aerial images. Some visual results are shown in Fig. 12.

For the evaluation on orientation prediction, our proposed Oriented RepPoints method achieves the best performance with 1.29° mAOE, which outperforms the state-of-the-art detectors like S²A-Net [12] and RoI-Trans. [10].

3) *Results on UCAS-AOD*: The UCAS-AOD dataset contains a large number of small objects, which are often overwhelmed by complex surrounding scenes in aerial images. For fair comparison, we report the results under AP₅₀ and AP₇₅. Table IX shows the evaluation results with the recent methods on UCAS-AOD dataset. It can be clearly seen that our presented method achieves the best performance of 90.11% AP₅₀ and 56.75% AP₇₅, respectively. Our proposed method achieves 89.51% AP₅₀ in the car detection, and obtains 90.70% AP₅₀ on airplane. The adaptive points as a fine-grained representation is able to capture the key points feature of small objects while the coarse representation of OBB is hard to extract abundant information for the detailed feature presentation of small objects. Fig. 13 gives some example detection results on UCAS-AOD dataset.

For the orientation evaluation, our method achieves the best orientation prediction results with 1.61° mAOE, which is lower than FR-O [20] and RoI-Trans. [10]. This demonstrates that our presented method is effective for the small aerial objects.

D. Discussion

In our proposed approach, the point set moves toward the appropriate position with the detailed geometric structure and semantic feature for the oriented objects, which are driven by both localization loss and classification loss simultaneously. Once the positions of the learned points are determined, the whole oriented box for object is directly estimated by the oriented conversion function. Such scheme is able to effectively avoid the ambiguity of regression target that commonly occurs in the conventional OBB-based approaches [8], [25].



Fig. 12. Sample object detection results of our proposed Oriented RepPoints method on HRSC2016 dataset.

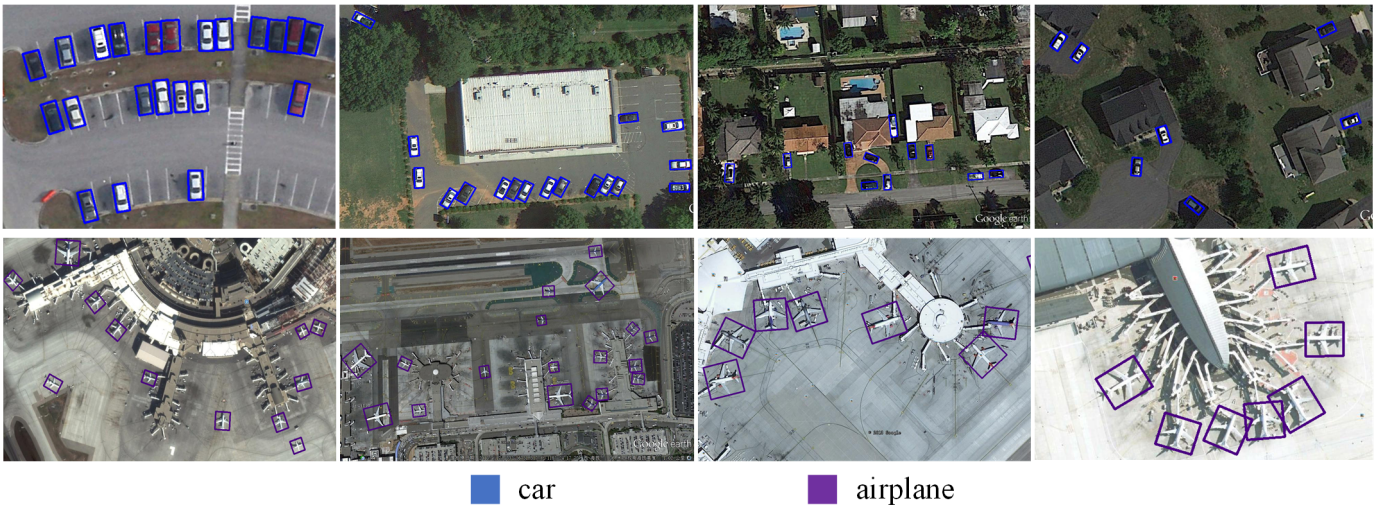


Fig. 13. Sample object detection results of our proposed Oriented RepPoints method on UCAS-AOD dataset.

Although having achieved encouraging results on the densely distributed objects with various orientations, our method may not perform well on the categories of large target, such as ground track field and soccer ball field. For future work, we will address this issue by incorporating more points in order to effectively capture the underlying semantic information over various levels of granularity.

V. CONCLUSION

This paper proposed a novel aerial object detector, which employed a set of adaptive points as a fine-grained representation for the oriented targets. Moreover, our method was capable of capturing the key semantic and geometric feature

for arbitrary-oriented, slender and cluttered objects in aerial image. We introduced an effective quality assessment measure to choose the high-quality point set samples for training. Furthermore, we imposed a spatial constraint on the points outside the bounding box to achieve robust adaptive point set learning. Additionally, we proposed a new metric to evaluate the orientation errors for the oriented object detectors. We have conducted the extensive experiments on three widely used testbeds for aerial object detection, whose promising results demonstrate that our proposed approach is effective.

REFERENCES

[1] G. Cheng, P. Zhou, and J. Han, "Learning rotation-invariant convolutional neural networks for object detection in vhr optical remote sensing

- images,” *IEEE Trans. Geosci. Remote Sens.*, vol. 54, no. 12, pp. 7405–7415, Dec. 2016.
- [2] K. Li, G. Wan, G. Cheng, L. Meng, and J. Han, “Object detection in optical remote sensing images: A survey and a new benchmark,” *ISPRS J. of Photogramm. Remote Sens.*, vol. 159, pp. 296–307, Jan. 2020.
- [3] P. Wang, X. Sun, W. Diao, and K. Fu, “Fmssd: Feature-merged single-shot detection for multiscale objects in large-scale remote sensing imagery,” *IEEE Trans. Geosci. Remote Sens.*, vol. 58, no. 5, pp. 3377–3390, Dec. 2020.
- [4] J. Pang, C. Li, J. Shi, Z. Xu, and H. Feng, “ \mathcal{R}^2 -cnn: Fast tiny object detection in large-scale remote sensing images,” *IEEE Trans. Geosci. Remote Sens.*, vol. 57, no. 8, pp. 5512–5524, Aug. 2019.
- [5] R. Dong, D. Xu, J. Zhao, L. Jiao, and J. An, “Sig-nms-based faster r-cnn combining transfer learning for small target detection in vhr optical remote sensing imagery,” *IEEE Trans. Geosci. Remote Sens.*, vol. 57, no. 11, pp. 8534–8545, Nov. 2019.
- [6] X. Yang, J. Yang, J. Yan, Y. Zhang, T. Zhang, Z. Guo, X. Sun, and K. Fu, “Scredet: Towards more robust detection for small, cluttered and rotated objects,” in *Proc. IEEE/CVF Int. Conf. Comput. Vis. (ICCV)*, Oct. 2019, pp. 8232–8241.
- [7] Y. Xu, M. Fu, Q. Wang, Y. Wang, K. Chen, G.-S. Xia, and X. Bai, “Gliding vertex on the horizontal bounding box for multi-oriented object detection,” *IEEE Trans. Pattern Anal. Mach. Intell.*, pp. 1–1, Feb. 2020.
- [8] J. Wang, W. Yang, H.-C. Li, H. Zhang, and G.-S. Xia, “Learning center probability map for detecting objects in aerial images,” *IEEE Trans. Geosci. Remote Sens.*, pp. 1–17, Jul. 2020.
- [9] G. Zhang, S. Lu, and W. Zhang, “Cad-net: A context-aware detection network for objects in remote sensing imagery,” *IEEE Trans. Geosci. Remote Sens.*, vol. 57, no. 12, pp. 10 015–10 024, Dec. 2019.
- [10] J. Ding, N. Xue, Y. Long, G.-S. Xia, and Q. Lu, “Learning roi transformer for oriented object detection in aerial images,” in *Proc. IEEE/CVF Conf. Comput. Vis. Pattern Recognit. (CVPR)*, Jun. 2019, pp. 2849–2858.
- [11] K. Fu, Z. Chang, Y. Zhang, G. Xu, K. Zhang, and X. Sun, “Rotation-aware and multi-scale convolutional neural network for object detection in remote sensing images,” *ISPRS J. of Photogramm. Remote Sens.*, vol. 161, pp. 294–308, Mar. 2020.
- [12] J. Han, J. Ding, J. Li, and G.-S. Xia, “Align deep features for oriented object detection,” *IEEE Trans. Geosci. Remote Sens.*, pp. 1–11, Mar. 2021.
- [13] F. Yang, W. Li, H. Hu, W. Li, and P. Wang, “Multi-scale feature integrated attention-based rotation network for object detection in vhr aerial images,” *Sensors*, vol. 20, no. 6, p. 1686, Mar. 2020.
- [14] X. Yang and J. Yan, “Arbitrary-oriented object detection with circular smooth label,” in *Proc. Eur. Conf. Comput. Vis. (ECCV)*, Aug. 2020, pp. 677–694.
- [15] M. Everingham, L. Gool, C. K. Williams, J. Winn, and A. Zisserman, “The pascal visual object classes (voc) challenge,” *Int. J. of Comput. Vis.*, vol. 88, no. 2, pp. 303–338, Sep. 2009.
- [16] K. Fu, Z. Chang, Y. Zhang, and X. Sun, “Point-based estimator for arbitrary-oriented object detection in aerial images,” *IEEE Trans. Geosci. Remote Sens.*, pp. 1–18, Sep. 2020.
- [17] H. Wei, Y. Zhang, Z. Chang, H. Li, H. Wang, and X. Sun, “Oriented objects as pairs of middle lines,” *ISPRS J. of Photogramm. Remote Sens.*, vol. 169, pp. 268–279, Nov. 2020.
- [18] Z. Yang, S. Liu, H. Hu, L. Wang, and S. Lin, “Reppoints: Point set representation for object detection,” in *Proc. IEEE/CVF Int. Conf. Comput. Vis. (ICCV)*, Oct. 2019, pp. 9657–9666.
- [19] Y. Chen, Z. Zhang, Y. Cao, L. Wang, S. Lin, and H. Hu, “Reppoints v2: Verification meets regression for object detection,” in *Proc. NIPS*, Dec. 2020, pp. 5621–5631.
- [20] G.-S. Xia, X. Bai, J. Ding, Z. Zhu, S. Belongie, J. Luo, M. Datcu, M. Pelillo, and L. Zhang, “Dota: A large-scale dataset for object detection in aerial images,” in *Proc. IEEE/CVF Conf. Comput. Vis. Pattern Recognit. (CVPR)*, Jun. 2018, pp. 3974–3983.
- [21] Z. Liu, L. Yuan, L. Weng, and Y. Yiping, “A high resolution optical satellite image dataset for ship recognition and some new baselines,” in *Proc. 6th Int. Conf. Pattern Recognit. Appl. Methods (ICPRAM)*, 2017, pp. 324–331.
- [22] H. Zhu, X. Chen, W. Dai, K. Fu, Q. Ye, and J. Jiao, “Orientation robust object detection in aerial images using deep convolutional neural network,” in *Proc. IEEE Int. Conf. Image Process. (ICIP)*, Sep. 2015, pp. 3735–3739.
- [23] X. Yang, H. Sun, K. Fu, J. Yang, X. Sun, M. Yan, and Z. Guo, “Automatic ship detection in remote sensing images from google earth of complex scenes based on multiscale rotation dense feature pyramid networks,” *Remote Sens.*, vol. 10, no. 1, p. 132, Jan. 2018.
- [24] S. M. Azimi, E. Vig, R. Bahmanyar, M. Körner, and P. Reinartz, “Towards multi-class object detection in unconstrained remote sensing imagery,” in *Proc. Asian Conf. Comput. Vis. (ACCV)*, Dec. 2018, pp. 150–165.
- [25] W. Qian, X. Yang, S. Peng, Y. Guo, and C. Yan, “Learning modulated loss for rotated object detection,” *arXiv preprint arXiv:1911.08299*, 2019. [Online]. Available: <http://arxiv.org/abs/1911.08299>
- [26] J. Wang, J. Ding, H. Guo, W. Cheng, T. Pan, and W. Yang, “Mask obb: A semantic attention-based mask oriented bounding box representation for multi-category object detection in aerial images,” *Remote Sens.*, vol. 11, no. 24, p. 2930, Dec. 2019.
- [27] X. Yang, Q. Liu, J. Yan, and A. Li, “R3det: Refined single-stage detector with feature refinement for rotating object,” *arXiv preprint arXiv:1908.05612*, 2019. [Online]. Available: <http://arxiv.org/abs/1908.05612>
- [28] Z. Liu, H. Wang, L. Weng, and Y. Yang, “Ship rotated bounding box space for ship extraction from high-resolution optical satellite images with complex backgrounds,” *IEEE Trans. Geosci. Remote Sens. Lett.*, vol. 13, no. 8, pp. 1074–1078, May. 2016.
- [29] S. Ren, K. He, R. Girshick, and J. Sun, “Faster r-cnn: Towards real-time object detection with region proposal networks,” *IEEE Trans. Pattern Anal. Mach. Intell.*, vol. 39, no. 6, pp. 1137–1149, Jun. 2017.
- [30] T.-Y. Lin, P. Dollár, R. Girshick, K. He, B. Hariharan, and S. Belongie, “Feature pyramid networks for object detection,” in *Proc. IEEE/CVF Conf. Comput. Vis. Pattern Recognit. (CVPR)*, Jul. 2017, pp. 936–944.
- [31] X. Wang, K. Chen, Z. Huang, C. Yao, and W. Liu, “Point linking network for object detection,” *arXiv preprint arXiv:1706.03646*, 2017. [Online]. Available: <http://arxiv.org/abs/1706.03646>
- [32] H. Law and J. Deng, “Cornernet: Detecting objects as paired keypoints,” in *Proc. Eur. Conf. Comput. Vis. (ECCV)*, Sep. 2018, pp. 734–750.
- [33] Z. Yang, Y. Xu, H. Xue, Z. Zhang, R. Urtasun, L. Wang, S. Lin, and H. Hu, “Dense reppoints: Representing visual objects with dense point sets,” in *Proc. Eur. Conf. Comput. Vis. (ECCV)*, Aug. 2020, pp. 227–244.
- [34] T.-Y. Lin, M. Maire, S. J. Belongie, J. Hays, P. Perona, D. Ramanan, P. Dollár, and C. L. Zitnick, “Microsoft coco: Common objects in context,” in *Proc. Eur. Conf. Comput. Vis. (ECCV)*, Sep. 2014, pp. 740–755.
- [35] S. Zhang, C. Chi, Y. Yao, Z. Lei, and S. Z. Li, “Bridging the gap between anchor-based and anchor-free detection via adaptive training sample selection,” in *Proc. IEEE/CVF Conf. Comput. Vis. Pattern Recognit. (CVPR)*, Jun. 2020, pp. 9759–9768.
- [36] H. Li, Z. Wu, C. Zhu, C. Xiong, R. Socher, and L. S. Davis, “Learning from noisy anchors for one-stage object detection,” in *Proc. IEEE/CVF Conf. Comput. Vis. Pattern Recognit. (CVPR)*, Jun. 2020, pp. 10 588–10 597.
- [37] K. Kim and H. S. Lee, “Probabilistic anchor assignment with iou prediction for object detection,” in *Proc. Eur. Conf. Comput. Vis. (ECCV)*, Aug. 2020, pp. 355–371.
- [38] X. Zhang, F. Wan, C. Liu, R. Ji, and Q. Ye, “Freeanchor: Learning to match anchors for visual object detection,” in *Proc. NIPS*, Dec. 2019, pp. 147–155.
- [39] X. Zhang, F. Wan, C. Liu, X. Ji, and Q. Ye, “Learning to match anchors for visual object detection,” *IEEE Trans. Pattern Anal. Mach.*, pp. 1–1, Jan. 2021.
- [40] D. A. Reynolds, “Gaussian mixture models,” *Encyclopedia of Biometrics*, pp. 659–663, 2009.
- [41] X. Zhou, J. Zhuo, and P. Krahenbuhl, “Bottom-up object detection by grouping extreme and center points,” in *Proc. IEEE/CVF Conf. Comput. Vis. Pattern Recognit. (CVPR)*, Jun. 2019, pp. 850–859.
- [42] Z. Guo, C. Liu, X. Zhang, J. Jiao, X. Ji, and Q. Ye, “Beyond bounding-box: Convex-hull feature adaptation for oriented and densely packed object detection,” in *Proc. IEEE/CVF Conf. Comput. Vis. Pattern Recognit. (CVPR)*, Jun. 2021.
- [43] T.-Y. Lin, P. Goyal, R. Girshick, K. He, and P. Dollár, “Focal loss for dense object detection,” *IEEE Trans. Pattern Anal. Mach. Intell.*, vol. 42, no. 2, pp. 318–327, Feb. 2020.
- [44] H. Rezaatofighi, N. Tsoi, J. Gwak, A. Sadeghian, I. Reid, and S. Savarese, “Generalized intersection over union: A metric and a loss for bounding box regression,” in *Proc. IEEE/CVF Conf. Comput. Vis. Pattern Recognit. (CVPR)*, Jun. 2019, pp. 658–666.
- [45] H. Fan, H. Su, and L. Guibas, “A point set generation network for 3d object reconstruction from a single image,” in *Proc. IEEE/CVF Conf. Comput. Vis. Pattern Recognit. (CVPR)*, Jul. 2017, pp. 2463–2471.
- [46] G. Cheng and J. Han, “A survey on object detection in optical remote sensing images,” *ISPRS J. of Photogramm. Remote Sens.*, vol. 117, no. 117, pp. 11–28, Jul. 2016.

- [47] K. He, X. Zhang, S. Ren, and J. Sun, "Deep residual learning for image recognition," in *Proc. IEEE/CVF Conf. Comput. Vis. Pattern Recognit. (CVPR)*, Jun. 2016, pp. 770–778.
- [48] X. Pan, Y. Ren, K. Sheng, W. Dong, H. Yuan, X. Guo, C. Ma, and C. Xu, "Dynamic refinement network for oriented and densely packed object detection," in *Proc. IEEE/CVF Conf. Comput. Vis. Pattern Recognit. (CVPR)*, Jun. 2020, pp. 11 207–11 216.
- [49] A. Newell, K. Yang, and J. Deng, "Stacked hourglass networks for human pose estimation," in *Proc. Eur. Conf. Comput. Vis. (ECCV)*, Oct. 2016, pp. 483–499.
- [50] J. Yi, P. Wu, B. Liu, Q. Huang, H. Qu, and D. N. Metaxas, "Oriented object detection in aerial images with box boundary-aware vectors," *Proc. IEEE/CVF Winter Conf. Appl. of Comput Vis (WACV)*, pp. 2150–2159, Mar. 2020.
- [51] A. P. Dempster, N. M. Laird, and D. B. Rubin, "Maximum likelihood from incomplete data via the em algorithm," *J. of the Royal Statist. Society Series B-method.*, vol. 39, no. 1, pp. 1–22, 1977.
- [52] Z. Zhang, W. Guo, S. Zhu, and W. Yu, "Toward arbitrary-oriented ship detection with rotated region proposal and discrimination networks," *IEEE Trans. Geosci. Remote Sens. Lett.*, vol. 15, no. 11, pp. 1745–1749, Aug. 2018.
- [53] J. Ma, W. Shao, H. Ye, L. Wang, H. Wang, Y. Zheng, and X. Xue, "Arbitrary-oriented scene text detection via rotation proposals," *IEEE Trans. on Multimedia*, vol. 20, no. 11, pp. 3111–3122, Mar. 2018.
- [54] M. Liao, Z. Zhu, B. Shi, G. Song Xia, and X. Bai, "Rotation-sensitive regression for oriented scene text detection," in *Proc. IEEE/CVF Conf. Comput. Vis. Pattern Recognit. (CVPR)*, Jun. 2018, pp. 5909–5918.
- [55] J. Redmon and A. Farhadi, "Yolov3: An incremental improvement." *arXiv preprint arXiv:1804.02767*, 2018. [Online]. Available: <http://arxiv.org/abs/1804.02767>